DE GRUYTER OPEN

Acta Geophysica
vol. 64, no. 5, Oct. 2016, pp. 1257-1274
DOI: 10.1515/acgeo-2015-0056

Three Dimensional Crustal Density Structure of Central Asia and its Geological Implications

Wencai YANG[2], Zhaoxi CHEN[1], Zunze HOU[2], and Changqing YU[2]

[1]Key Laboratory of Geo-detection, China University of Geosciences, Ministry of Education, Beijing, China

[2]Institute of Geology, Chinese Academy of Geological Sciences, Beijing, China
e-mail: zxchen@cugb.edu.cn (corresponding author)

A b s t r a c t s

This paper introduces the scale-depth law of multi-scale wavelet analysis for regional gravity data processing, and presents the results of its application to Central Asia for computation of the 3D crustal density structures. The wavelet analysis method is applied for characterizing 3D crustal density structure, producing five maps of density disturbance corresponding to different depths of equivalent layers in the crust. The results provide important evidence for the study of crustal structures and mass movement in Central Asia: (i) the small-scale and intensive linear density disturbances in the upper crust indicate Phanerozoic orogenic belts; (ii) there exists a horseshoe-shaped low-density belt in the middle crust coinciding with the Kazakhstan orocline; (iii) there is a very low density zone in the lower crust, extending from western Kunlun to Tianshan, probably indicating a lower-crust flow; (iv) there are a few low-density spots in the middle crust, which might be caused by low-density mass squeezing upward from the lower crust flows.

Key words: Central Asia, multi-scale wavelet analysis, density disturbance, lower-crust flows, orocline.

1. INTRODUCTION

Central Asia is the converging region of the Paleo-Asian Ocean and has important significance for the study of ocean-continent transition, continental accretion and the formation of Pangea supercontinent. Since the Cenozoic, Central Asia has become reactive in its lithosphere owing to the collision between the India and Eurasia plates, so important in the study of long-distance effects of the continental collision.

Regional gravity field on the continent, including the free air anomalies, can partly indicate the crustal structures. Previous studies (Artemjev *et al*. 1994) have shown that variations of crustal thickness in Central Asia can only provide 30-50% compensation of the Earth's gravitational equilibrium, and the remaining 50-70% of the compensation is due to crustal density inhomogeneity, which is mainly relevant to crustal structures, lithological variations, and the degree of fluid filling. After performing terrain and middle layer correction, Bouguer anomalies mainly reflect crustal structures, lithological variations and the degree of fluid filling in different depths of crust. So the imaging of three-dimensional crustal density structures can be a good way to reveal the crustal structures and tectonic events.

After years of researches, we have combined some tested data-processing techniques, including the multi-scale wavelet analysis, harmonic analysis and inversion of density disturbance, into a gravity data-processing system that is applicable for delineation of three dimensional crustal density structures. This system is referred to as multi-scale analysis of regional gravity field (Hou and Yang 1997, 1998; Yang *et al*. 2001, 2005; Yang and Yu 2014a). In the papers listed above, we introduce how to construct special wavelet base for regional gravity data processing, the multi-scale analysis for three-dimensional crustal density structures with some equivalent layers, as well as their applications in China mainland, Tibet Plateau and Australia. Achieving good results of the multi-scale wavelet analysis comes from the relation between the horizontal scale of gravity field and the buried depth of sources, which is called scale-depth conversion law for regional Bouguer gravity field. Starting from the scale-depth conversion law, this paper introduces the three dimensional imaging results of crustal density structures applied to the Central Asia region, and analyzes the geodynamic meanings of the corresponding research results .

2. SCALE-DEPTH CONVERSION LAW OF MULTI-SCALE WAVELET ANALYSIS FOR BOUGUER GRAVITY FIELD

The basis of the multi-scale wavelet analysis for regional gravity data processing is that the horizontal scale of gravity anomalies is proportional to the buried depth of the gravity sources. In other words, the deeper the source

buries, the larger the horizontal scale of the anomaly becomes. For instance, the gravity anomaly of a sphere object can be written as (Telford *et al*. 1990)

$$\Delta g = \frac{GMh}{\left(x^2 + h^2\right)^{3/2}} , \tag{1}$$

where G is the gravitational constant, M is the mass of the sphere, h is the depth of the sphere center, and x is the horizontal distance from observed points to the projection of the sphere center on the observation plane.

Define the horizontal width of gravity anomaly W satisfying $W = 2x'$, in which x' is the horizontal distance between the origin to the point where the maximum anomalous values attenuate to the half. Then W also represents characteristic scale of the isolated anomaly. Substituting x' into Eq. 1 yields

$$h = \frac{x'}{\sqrt{2^{2/3} - 1}} = 1.305x' = 0.6525W = \alpha W . \tag{2}$$

Thus, the deeper the field source buries, the larger the horizontal scale of the anomaly becomes. The buried depth and the horizontal scale are approximately proportional to each other. Nevertheless, due to the different shapes of buried sources, the scaling factor α may vary with source shapes, satisfying the condition $\alpha = 0.2\text{-}0.9$. For instance, the value of α can be chosen as 0.8 for intrusive thin dykes.

When the gravity anomalies are produced by the superposition of several field sources, they will no longer have similar characteristic scales with Eq. 2. Specifically, the characteristic scale W for the spherical source with the center depth of 4 km in upper crust is 6.13, and that with the center depth of 34 km in lower crust is 52.1. However, the scale may range from 6 km to 52 km when the above two anomalies are added together, indicating no characteristic scale after the superposition. The multi-scale wavelet analysis utilizes the characteristic scale of the desired wavelet base to recover the characteristic scale in the ground superimposed anomalies, and decomposes them with different scales, making the decomposed wavelet details to obtain characteristic scales again. For the above example, the superimposed anomalies are decomposed by the wavelet analysis with the wavelet scale of 6, 12, 24, and 48 km. The first-order wavelet detail D1 with the scale of 6 km extracts the anomaly field produced by the spherical source buried with the center depth of 4 km in the upper crust. The fourth-order wavelet detail D4 with the wavelet scale of 48 km draws the anomaly produced by the spherical source buried with the center depth of 32 km in the lower crust. In a certain sense, the wavelet details can restore the characteristic scale in gravity field. Therefore, the multi-scale wavelet analysis can be an important technology for delineating three-dimensional crustal density structures.

Assume the gravity data spacing in a uniform square grid as Δ. When applying the conventional wavelet multi-scale analysis, the wavelet base will take 4 sampling points (Mallat 1989), with the shape of peaks and valleys and the characteristic scale of about half of the peak width, namely Δ/2. The scale of the wavelet details increases with the power of 2 during wavelet transforms. Defining the order of the wavelet details as n, the characteristic scale of n-order wavelet details can be written as

$$L_n = \Delta \cdot 2^n / 2 = \Delta \cdot 2^{n-1}, \quad n = 1, 2, 3, \ldots . \tag{3}$$

The multi-scale wavelet analysis requires the characteristic scale L_n of wavelet details should match with the scale W of the gravity anomalies. Substituting Eq. 3 into 2, gives

$$\alpha = h / L_n \tag{4}$$

and

$$h = \alpha \cdot \Delta \cdot 2^{n-1}, \quad n = 1, 2, 3, \ldots , \tag{5}$$

Equation 5 represents the relation between the buried depth h of field sources and the n-order wavelet details, namely the scale-depth conversion law in the multi-scale wavelet analysis for decomposition of Bouguer gravity field. For some ground gravity data sets with different observed meshes or survey scales, the characteristic scales of wavelet details are estimated by Eq. 3 and listed in Table 1. The gravity data sets with the sampling spacing greater than 10 km cannot be suitable for multi-scale wavelet analysis and three-dimensional characterization of fine crustal density structures. However, if the sampling spacing is less than 1 km, the result can only be valid for the decomposition of the upper crust because of too small scale of wavelet details.

Table 1

Characteristic scales of wavelet details from wavelet transform

Survey scale	1:10 000	1:200 000	1:800 000	1:2 000 000
Δ	0.1 km	2 km	8 km	20 km
Order n = 1	0.1	2	8	20
2	0.2	4	16	40
3	0.4	8	32	80
4	0.8	16	64	160
5	1.6	32	128	320
6	3.2	64	256	640
7	6.4	128	512	1280

Note: Δ represents data spacing, the scales marked with underline are not suitable for gravity decomposition and multi-scale wavelet analysis.

In advance, one may use the Eq. 4 to estimate the buried depth of gravity sources related to the wavelet details. For example, a regional data set with the survey scale of 1:500 000 or 1:1 000 000 can be interpolated into a grid with the mesh interval of 4-10 km. In this situation, the scale of the wavelet detail D1 is 2 km, and the scale of the n-order wavelet details corresponds with 2^n km. The buried depth of field source in accordance with the wavelet details can be estimated by formula 5 after selecting the coefficient α; the results are shown in Table 2. Table 2 also gives buried depth estimations of wavelet details corresponding to the upper, middle, and lower crust as well as possible combinations of wavelet details in the process for crustal density imaging. To be specific, (D1 + D2) can be used for inversion of density disturbance for shallow sedimentary basins, (D3 + D4) for deep layers of sedimentary basins or crystal basements in the upper crust, (D5 + D6) for the middle crust, and so on. Note that the buried depths shown in Table 2 can be too rough because gravity anomalies changes in different areas greatly; one should not treat these value as the exact buried depths of the equivalent layers that correspond to a certain wavelet detail.

Table 2

Referent buried depth estimations of the wavelet details (data spacing: 4~8 km)

Details' order 2^n	Characteristic scale [km]	Selected coefficient α	Buried depth of field sources [h /km]	Combined details
D1--2^1	2	0.8	1.6	D1+D2: sedimentary basins
D2--2^2	4	0.75	3.0	
D3--2^3	8	0.69	5.52 (shallow layer in upper crust)	D3+D4:
D4--2^4	16	0.62	9.92 (crystalline basement in upper crust)	
D5--2^5	32	0.54	17.3 (upper-middle crust)	D5+D6:
D6--2^6	64	0.41	26.2 (middle-lower crust)	
D7--2^7	128	0.3	38.4 (lower crust)	

The exact average buried depths should be calculated by the slope of the power spectrum of the wavelet details according to the spectral analysis of the gravity anomalies (Spector and Grant 1970). Experiments show that the

buried depths of the equivalent layers calculated by the power spectrum may differ from Table 2, especially for non-square gridding data.

In summary, the deeper the geological source buries, the larger the horizontal scale of gravity anomalies as well as the density disturbance have. So after multi-scale wavelet decomposition of gravity data, small-scale wavelet details indicate density distribution of shallow sources, whereas large-scale wavelet details represent the distribution of deep sources. Since we presented multi-scale wavelet analysis for gravity data processing, the method has already shown good results (Hou and Yang 1997, 1998, 2011; Yang *et al*. 2001, 2005, Yang and Yu 2014a, b).

3. MULTI-SCALE DECOMPOSITION OF THE REGIONAL GRAVITY FIELD IN CENTRAL ASIA

Revealing the three dimensional crustal density structures from regional gravity field has become one of the research frontiers in the recent years. In the beginning of 21th century, the Ministry of Land and Resources has completed 1:1 000 000 regional ground gravity survey in most regions in Chinese continent. Oil companies and our group also have been carrying out complementary gravity surveys in some focus areas. All surface gravity data sets are compiled and the location of the observation stations is shown in Fig. 1a. The Bouguer gravity data sets in the whole Central Asia are obtained after combination of the ground data and satellite data together with some special procedures. The studied area covers the range of latitude 33°-50°, longitude 70°-100°, and the data sets are interpolated into 5 km × 5 km grid (shown in Fig. 1b).

The multi-scale analysis is composed of four modules, including the division and depth estimation of gravity sources, the multi-scale wavelet analysis, the depth estimation of wavelet details and inversion of density disturbance. The first question is: how many equivalent layers of gravity sources can be made? We can perform the spectral analysis of the regional gravity field to see how many segments with different slopes in the power spectrum. According to the theory of the gravity anomalies in the wavenumber domain (Bhimasankakam *et al*. 1977, Yang and Guo 1979, Yang 1985), these segments with different slopes in the power spectrum indicate the equivalent layers with different depths of buried sources. Because there are six distinguished segments exhibiting in the power spectrum of gravity field of the studied area, the regional gravity field should be divided into seven equivalent layers. Moreover, the Mallat algorithm is applied to construct a particular wavelet bases for the separation of gravity anomaly and the multi-scale wavelet analysis (Mallat 1989, Hou and Yang 1997, 1998, 2011). The wavelet details from D1 to D8 are calculated and are formed into five abnormal subsets, *i.e.*, (D1 + D2), (D3 + D4), (D5 + D6), D7, and D8.

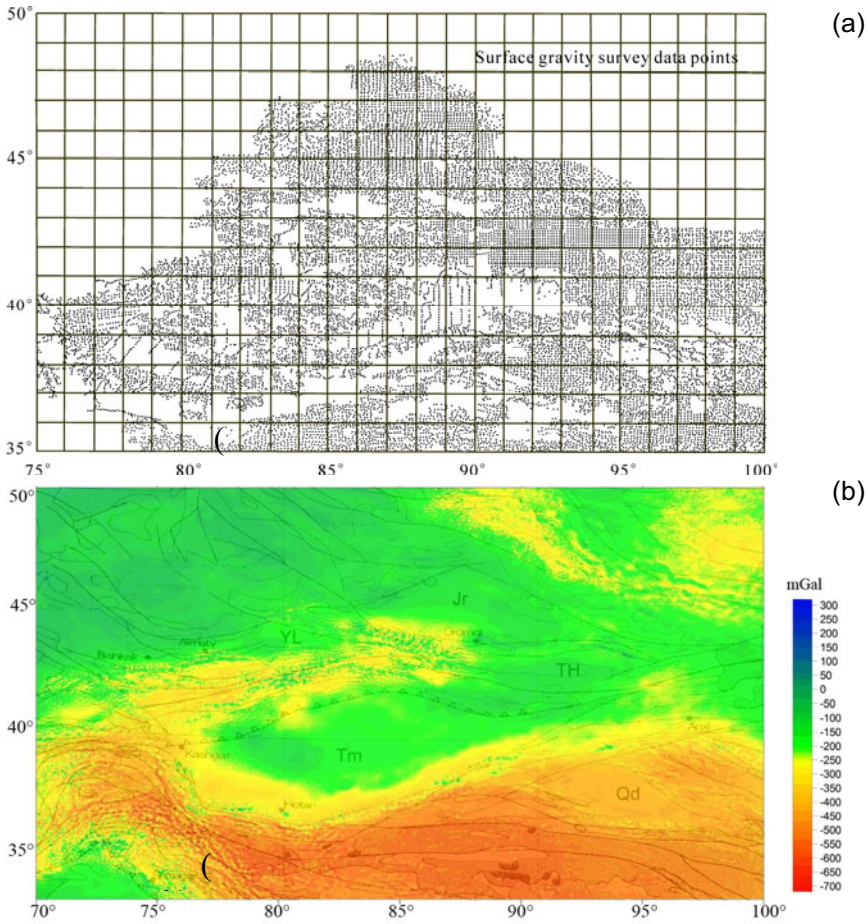

Fig. 1: (a) Distribution of surface gravity measurement stations in the studied area; (b) The Bouguer gravity anomalies obtained by combination of the surface and satellite data (Tm – Tarim, Qd – Qaidam, TH – Tuha, Jr – Junggar, and YL – Yili).

The wavelet detail D2 corresponds to the shallowest layer as shown in Fig. 2a, and the details (D3 + D4) are shown in Fig. 2b.

The average buried depth of the equivalent layers corresponding to the five abnormal subsets can be calculated from the power spectrum slopes of the wavelet details. The calculated depth of the shallowest layer (D1 + D2) is 3 km, the shallow layer (D3 + D4) 10 km, the middle layer (D5 + D6) 18 km, the deep layer (D7) and deepest layer (D8) are about 30 and 48 km, respectively. The shallowest and shallow layers are located on the top of the upper crust and the crystalline basement, respectively. The middle is located in the bottom of the upper crust, the deep layer is located in the middle crust, and

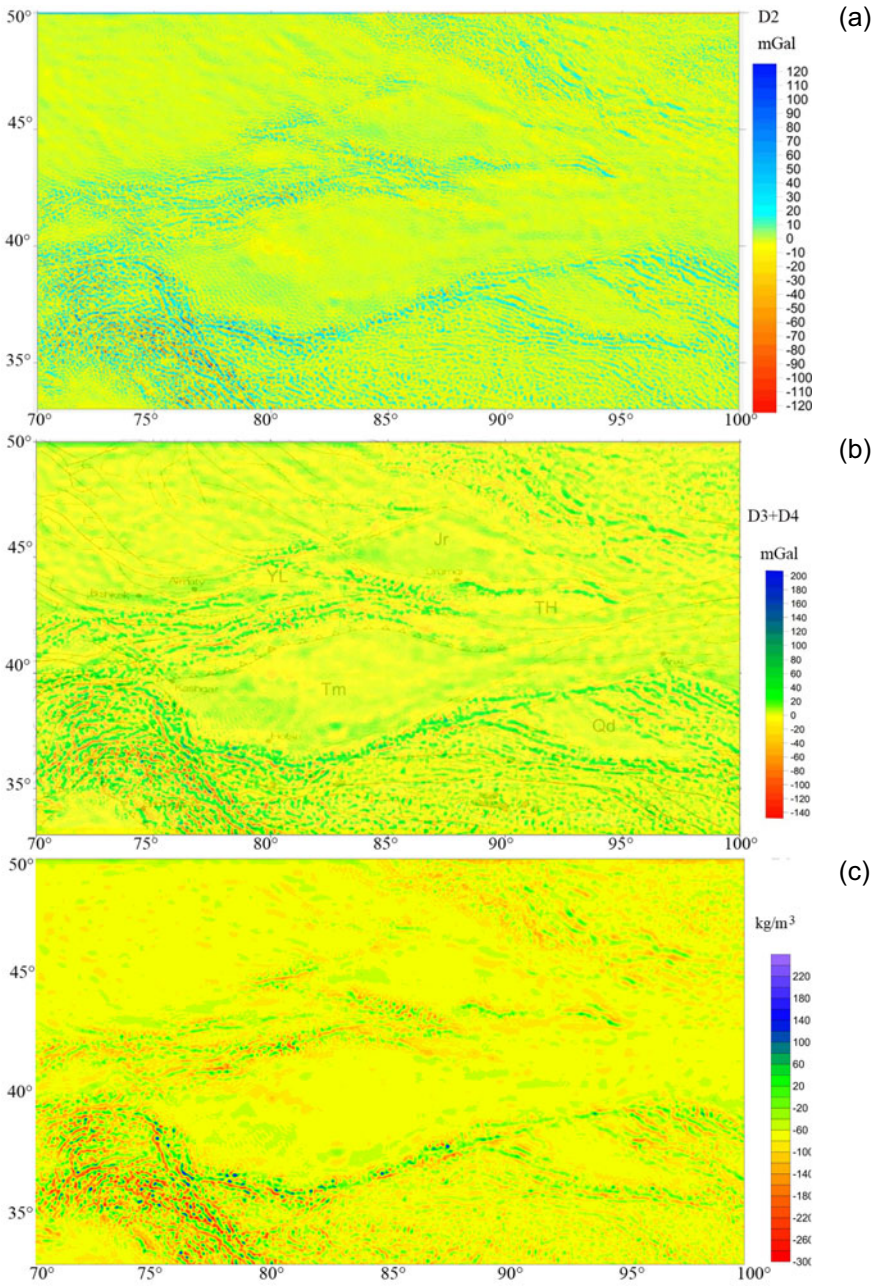

Fig. 2: (a) The 2nd order wavelet detail (D2) of the Bouguer gravity anomalies; (b) The 3rd and 4th order wavelet details (D3 + D4) of the Bouguer gravity anomalies refer to the equivalent layer of average depth 10 km; (c) The density disturbance from wavelet details (D3 + D4) refers to the equivalent layer of average depth 10 km.

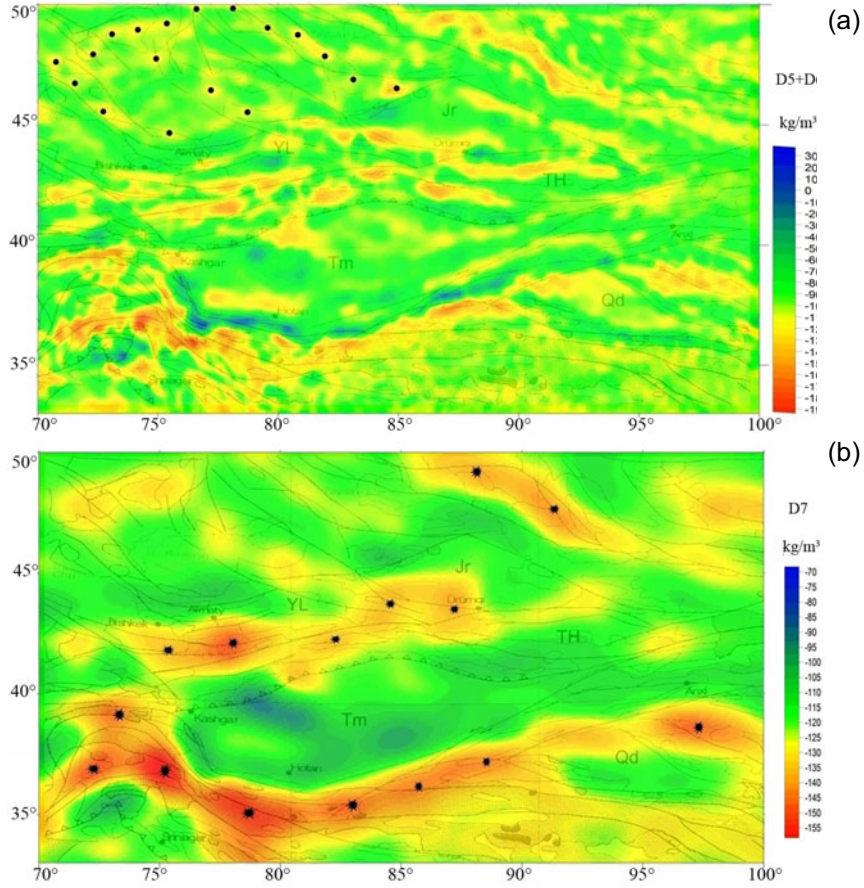

Fig. 3: (a) The density disturbance from wavelet details (D5 + D6) refers to the equivalent layer of average depth of 18 km; black dots indicate the Kazakhstan orocline; (b) The density disturbance from wavelet detail (D7) refers to the equivalent layer of average depth 30 km; black stars indicate the heavy low-density zones.

the lowest is located in the lower crust of the studied area. To study three dimensional crustal density structure, the generalized linear inversion is used to obtain the density disturbance of each equivalent layers after the completion of the multi-scale wavelet analysis and the estimation of depths. The density disturbance of equivalent layers refers to the difference between the average density of equivalent layers and the inversed density values at the depth. Assume that the average densities from the shallowest and middle equivalent layers in the upper crust are 2.65×10^3 and 2.81×10^3 kg/m^3, respectively. Also, the densities in the middle crust and lower crust are supposed to be 2.91×10^3 and 2.97×10^3 kg/m^3. The density disturbance of the

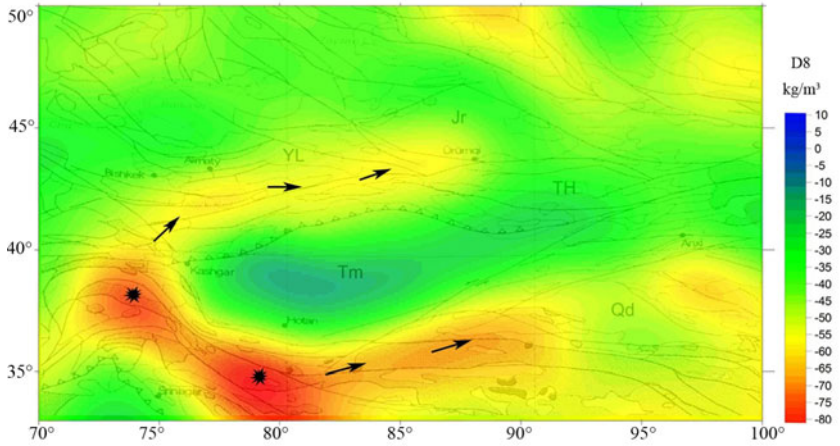

Fig. 4. The density disturbance from wavelet detail (D8) refers to the equivalent layer of average depth 48 km; black stars indicate the sources of the lower-crust channel flows, black arrows indicate the channel flows.

middle layer inversed from the wavelet details (D5 + D6) is shown in Fig. 3a, and that from (D7) and (D8), separately, representing the middle crust and lower crust are shown in Figs. 3b and 4.

4. THE VARIATIONS OF THE CRUSTAL DENSITY STRUCTURES IN CENTRAL ASIA

We obtained five density disturbance maps of the equivalent layers after applying the above-mentioned methods for three dimensional crustal density structures of Central Asia. The density disturbance map of the shallowest layer D1 is more or less in coincidence with the geological map, thus providing few information for crustal analysis. The most important maps we care about involve the maps corresponding to crystalline basement of the upper crust, to the middle crust, and lower crust. Because the behavior and properties of the upper, middle, and lower crust are quite different, rocks in the upper crust show the properties of brittle and easy to break, and rocks in the lower crust have lower viscosity coefficient, easy to form creeping flows (Jolivet and Hataf 2001, Kirby and Kronenberg 1987, Yang 2009). Under the temperature and pressure in the middle crust, rocks may have higher water-solution rate to be detached. Thus, there are many complex faults developed in the upper crust, but not many developed in the lower crust. As a result, the density disturbances and their corresponding structures can be quite different from the geological data in the surface.

4.1 Density disturbances in the upper crust

We firstly analyze structures of the upper crust from the density disturbance map from the wavelet details D2 shown in Fig. 2a. The map shows density disturbance of the equivalent layer with the average depth of 3 km. Because of low densities of sedimentary rocks, sedimentary basins are displayed as calm regions with less variation and small disturbance. The small-scale and strong anomalies are usually distributed along orogenic belts. The density disturbance map obtained from wavelet details (D3 + D4) are shown in Fig. 2c, with the average depth of about 10 km, indicating the density disturbance of the crystalline basement of the upper crust. The yellow and green area in the figure represents stable tectonic units where the variation of density disturbance is mild. The basins including Tarim (marked "Tm" in the figure), Qaidam (Qd), Tuha (TH), Junggar (Jr), and Yili (YL) belongs to basins of such a kind. The zones illustrated with blue or red color belts in the map show high density areas or low density areas, respectively. The dense areas with both blue and red dots indicate tectonically active zones or intensive deformation belts as the rock density varies dramatically. These areas in the map are located mainly in Kashmir, Tianshan Mountain, Mayili-Sawuer Mountain, Altai Mountain, East and West Kunlun Mountain, Altun Mountain, and Qinlian Mountain ranges. Kashmir shows the most violent deformation caused by collision between Indian plate and Eurasia plate in Cenozoic, resulting in dramatic density disturbances in the upper crust. All the above mentioned mountain ranges are orogenic belts formed in the late Paleozoic by the collision involving the Kazakhstan, Tarim, Qiangtang terranes as well as the Siberia and Sino-Korean Cratons (Artemjev *et al*. 1994, Abrajevitch *et al*. 2008, Yang 2009). They have also been under severe crustal deformation caused by the collision between the India plate and Eurasia plate in the Cenozoic (James 1989, Rogers 2004, Molnar 1988, Meissner and Mooney 1998, Xu *et al*. 2007, Xiao 2010, Yang and Yu 2014a, b; Royden *et al*. 1997). In short, the small-scale strong accumulating density disturbances of the upper crust indicate the Phanerozoic orogenic belt, and the density variations are consistent with the tectonic deformation and geological structures observed on the surface.

Figure 2c also shows that the density of the upper crust is not high in general, with the value of less than 2.65×10^3 kg/m^3 in the crystalline basement. We speculate that the reason of low density in the upper crust is associated with the existence of water that was saved from the Paleo-Asian ocean. The studied region was located in the center of the Paleo-Asian Ocean 3 Ma ago. Some water of the ocean might be infiltrated into the mantle, the other part might be penetrated into cracks of crustal rocks, making the crust full of water and decreasing its rock densities.

4.2 Density disturbance in the middle crust and the orocline

Figure 3a shows the density disturbance of the wavelet details (D5 + D6) with the equivalent layer depth of 18 km, indicating the density variations on the bottom of upper crust or the top of the middle crust. The color bar is still the same as mentioned in Section 4.1. The high density zones are mainly distributed in the southern part of Tarim Basin, while the intensive low density zones are located in the south, *i.e.*, West Kulun Mountain and Altun Moutain ranges. We can see that the south part of Tarim, like a rigid shield, resists against the strong compression from the Tibetan plateau since the Jurassic, making the basin saved, without being broken. The orognic belts of Tianshan Mountain, Kunlun Mountain, and Altun Mountain are presented as low density zones. Because of their granitite masses with relatively low density and possibly fluid composition, orogenic zones usually show low density disturbance together with many fracture and deformation belts in the middle crust.

The word "orocline" refers to sharp-bent folds and thrust belts produced by a series of deformations. The famous Kazakhstan horseshoe-shaped orocline is located in the northwest of the studied area (Abrajevitch *et al*. 2008, Xiao 2010). It was formed during closure of the ancient Asian ocean in the Late Paleozoic, indicating the split collision and rotary displacement of the blocks such as Siberia, the Baltic, and the Tarim. In Fig. 3a there is a combination of horseshoe-shaped belts with low density disturbance (marked with dot string), in coincidence with the location of Kazakhstan orocline. The amplitude of the low density disturbance in the horseshoe belts is not as strong as in the Kunlun orogenic belts, as it occurred earlier than the Mesozoic and Cenozoic orogenic belts such as Kunlun. The fact that the Kazakhstan orocline looms in the density disturbance map of the middle crust suggests that Paleozoic orogenic belts still have traces in the density structures in the middle crust, although their roots on the Moho discontinuity may be polished today. This example shows that the existence of low density disturbance in the middle crust can probably provide important evidence to identify whether there orocline exists.

Why does Kazakhstan orocline appear as a low density disturbance? From the view of tectonic evolution, there are two possible reasons. Firstly, the orocline involved with island arc belts was formed by subduction from Mongolia-Okhotsk Ocean to Kazakhstan in Permian (Abrajevitch *et al*. 2008, Xiao 2010). The island arc belts contained lots of active fluid saved in pores of andesite rocks, making the normal density decrease. Secondly, the Siberia craton, Kazakhstan and Tarim terranes collided in the region after the Permian. Strong collision not only caused the horseshoe-shaped bending of the Kazakhstan orocline, but also produced the crustal shorting and thickening and a density decrease of crustal rocks.

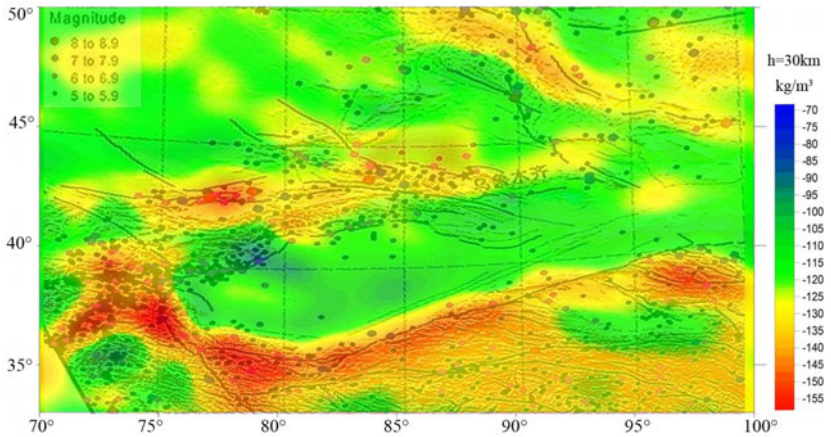

Fig. 5. Comparison between the density disturbance on the equivalent layer of average depth of 30 km and earthquakes with magnitude greater than 5.

Figure 3b shows the density disturbance of the wavelet details (D7) with the equivalent layer depth of 30 km, indicating the density variations in lower part of the middle crust. The high density zone marked with blue color is distributed below the Tarim Basin, especially in the north of Bachu uplift. However, both the inner part of Bachu uplift and the Tabei uplift have relatively lower density disturbance. Figure 3b shows that the lower density zones not only expand their areas, but are also connected into a series of round belts (illustrated by black stars) surrounding some high density blocks. These high density blocks include Tarim (Tm), Qaidam (Qd), Tuha (TH), Junggar (Jr), and Yili (YL), and demonstrate having craton attributes. The lower density zones are located in the area of the north and east edge of Kashmir, West Kunlun, Altan, Qilian, Altai, and Tianshan, which are also tectonic active zones containing intensive deformation belts (Nelson and Zhao 1996, Yang and Yu 2014a). Although they are different in ages, they have all become tectonically active again since the collision between India and Eurasian continents. Comparison between the density disturbance map with the locations of earthquakes is shown in Fig. 5. One can see that the earthquakes with the magnitude greater than 5 mainly occur in the middle crust at the lower density belts or their edges, indicating a causal relationship between crustal deformation and the density structures.

4.3 Density disturbances and channel flows in the lower crust

Figure 4 shows the density disturbance of the wavelet details (D8) with the equivalent layer depth of 48 km, indicating the density variations in the lower crust. The blue high density zone is distributed mainly in the Tarim

basin, extending from Bachu uplift to Tuha block. This may suggests some kind of relationship between these two oil and gas basins. The lowest density zone appears in the West Kunlun, and this solid terrane was the place of convergence of Tarim, Tibet, and Kazakhstan and undergone the collision processes (marked in black stars). Due to the collision and friction of several terranes, the temperature of the lower crust would rise and rocks might tend to partial melting and produce channel flows in the lower crust. Rocks could undergo creep motion rheologically and show lower density along some channels in the lower crust. The term of "channel flow" originally refers to movement of melting masses from or within the lower crust (Law *et al*. 2006, Clark and Royden 2000, Unsworth *et al*. 2005, Grujic 2006, Schoenbohm *et al*. 2006, Harris 2007, Zhao *et al.* 2008, Wang *et al*. 2007). We may expand its meaning to any rheological creep motion along some channels both in vertical and horizontal directions. Thus the low density disturbance belts in the lower crust must have tight relationship with the channel flow. The lower density anomalies of crustal rocks may be mainly caused by lithological variations, increasing some fluid substance, and changing temperature and pressure as well. The increasing temperature and fluid substance reduces rock densities, and also stimulates the crustal creep motion. Therefore, the results of three dimensional crustal density imaging can provide indirect evidence for the study of the channel flow in the lower crust.

From the latest research results of the Qinghai-Tibet Plateau, the flow in lower crust can be divided into vertical channel flow and lateral channel flow. The granite bodies in the high Himalaya orogenic belt, formed during post-collision (40-20 Ma), indicate vertical channel flow (Clark and Royden 2000, Unsworth *et al*. 2005, Zeng *et al*. 2011). This kind flow was generated by dehydrating sedimentary rocks in the middle-to-lower crust, and remelting upward. It coincides with local low density anomalies of small-scale in the middle and upper crust. The lateral channel flow is attributed to the partial melting of rocks due to penetration of the low density sea of ancient oceans subducting into the mantle. Water reduces the melting temperature of solid rocks after closure of the ancient oceans, causing partial melting and the lateral channel flow. The low density channels of large scales in the lower crust may reveal this type of flows.

The lateral channel flows of low density in the studied area are illustrated in Fig. 4 marked with black stars. They start from West Kunlun, then are divided into two branches, named the northern and southern, respectively, traveling from west to east (see the black arrows in the figure). The southern branch travels along Altun and is trending northeast; then it turns to southeast toward Qilian Mountain. The northern branch travels towards the northeast along South Tianshan, and then goes to North Tianshan and the south of Junggar Basin. The width of the lower density zone in the lower crust is of

about 230 km. We may treat the large scale lower density zones from West Kunlun to Tianshan as a lower-crust channel flow caused by long-distance effect of the collision between India and Eurasia plates. The southern branch of the flow is located along north-western Tibet Plateau and also relates to long-distance effect of the collision between India and Eurasia plates. Comparing the images shown in Figs. 2, 3, and 4, we see that the lower density disturbance zones gradually expand from the upper crust to the lower crust. The high density blocks are not only reduced in number, but also present more clear boundaries in favor of dividing crustal tectonic units.

5. CONCLUSIONS

The methods of the multi-scale wavelet analysis and inversion density disturbance are applied to characterize three dimensional crustal density structure producing five maps of density disturbance corresponding to different depths of equivalent layers in the crust. The research results provide important evidence for the study of crustal structures and mass movement in the studied area as follows:

- The scale of Bouguer gravity anomalies is approximately proportional with the buried depth of gravity sources. The deeper the sources locate, the larger the horizontal scales of gravity anomalies become;
- The small-scale and intensive linear density disturbances in the upper crust indicate Phanerozoic orogenic belts. The overall density of the upper crust in the studied region appears low in general, owing to closure of the Paleo-Asian Ocean;
- There exists a horseshoe-shaped low-density belt in the middle crust coinciding with the Kazakhstan orocline. The Siberia craton, the Kazakhstan and Tarim terranes collided in Permian, causing the horseshoe-shaped bending of the orocline and the crustal low density belt;
- There is a very low density zone in the lower crust, extending from western Kunlun to Tianshan, probably indicating a lower-crust flow. If one divides the flow into two categories, *i.e.*, vertical channel flow and lateral channel flow, the former belongs the lateral flow coming from the western Tibetan Plateau with a width of about 230 km;
- There are a few low-density spots in the middle crust, which might be caused by low-density mass squeezing upward from the lower crust flows. The locations of these zones coincide with earthquake focus (magnitude > 5), implicating that the movement of lower-crust flows may induce deformation in the middle crust, deducing the rock density as well.

Acknowledgements. This work was supported by the National Natural Science Foundation of China (No. 41304101), Chinese Geological Sur-

vey Project (12120113093800), the Fundamental Research Funds for the Central Universities (2-9-2013-47), and the Fundamental Research Fund (GDL1205) of Key Laboratory of Geo-detection and the open project of State Key Laboratory of Continental Tectonics and Dynamics (201302). The authors wish to thank the anonymous reviewers for their critical review of the manuscript and many helpful comments.

References

Abrajevitch, A., R. Van der Voo, M.L. Bazhenov, N.M. Levashova, and P.A. McCausland (2008), The role of Kazakhstan orocline in the late Paleozoic amalgamation of Eurasia, *Tectonophysics* **455**, 1-4, 61-76, DOI: 10.1016/j.tecto.2008.05.006.

Artemjev, M.E., M.K. Kaban, V.A. Kucherinenko, G.V. Demyanov, and V.A. Taranov (1994), Subcrustal density inhomogeneities of Northern Eurasia as derived from the gravity data and isostatic models of the lithosphere, *Tectonophysics* **455**, 1-4, 249-280, DOI: 10.1016/0040-1951(94)90275-5.

Bhimasankakam, V.L.S., A. Nagendra, and R. Seshagiri (1977), Interpretation of gravity anomalies due to finite inclined dikes using Fourier transformation, *Geophysics* **42**, 1, 51-59, DOI: 10.1190/1.1440713.

Clark, M.K., and L.H. Royden (2000), Topographic ooze: Building the eastern margin of Tibet by lower crustal flow, *Geology* **28**, 8, 703-706, DOI: 10.1130/0091-7613(2000)28<703:TOBTEM>2.0.CO;2.

Grujic, D. (2006), Channel flow and continental collision tectonics: an overview, *Geol. Soc. London* **268**, 25-37, DOI: 10.1144/GSL.SP.2006.268.01.02.

Harris, N. (2007), Channel flow and the Himalayan–Tibetan orogen: a critical review, *J. Geol. Soc.* **164**, 511-523, DOI: 10.1144/0016-76492006-133.

Hou, Z.Z., and W.C. Yang (1997), Two-dimensional wavelet transform and multiscale analysis of gravity field in China, *Chinese J. Geophys.* **40**, 2, 261-273.

Hou, Z.Z., and W.C. Yang (1998), Multi-scale inversion of density contrast within the crust of China, *Chinese J. Geophys.* **41**, 5, 642-651.

Hou, Z.Z., and W.C. Yang (2011), Multi-scale inversion of density structure from gravity anomalies in Tarim Basin, *Sci. China Earth Sci.* **54**, 3, 399-409, DOI: 10.1007/s11430-011-4169-2.

James, D.E. (1989), *Encyclopedia of Solid Earth Geophysics*, Van Nostrand Reinhold Co., New York,

Jolivet, L., and H.-C. Hataf (2001), *Geodynamics*, A.A. Balkema Pub., Lisse.

Kirby, S.H., and A.K. Kronenberg (1987), Rheology of the Lithosphere: selected topics, *Rev. Geophys*. **25**, 6, 1219-1224, DOI: 10.1029/RG025i006p01219.

Law, R.D., P. Searle, and L. Godin (2006), Channel flow, ductile extrusion and exhumation in continental collision zones, *Geol. Soc. Spec. Pub*. **268**, 91-145, DOI: 10.1144/GSL.SP.2006.268.01.01.

Mallat, S. (1989), Multifrequency channel decomposition and wavelet models, *IEEE Trans. Acoust. Speech Signal Proc.* **37**, 12, 2091-2110, DOI: 10.1109/29.45554.

Meissner, R., and W. Mooney (1998), Weakness of the lower continental crust: a condition for motions, uplift and escape, *Tectonophysics* **296**, 1-2, 47-60, DOI: 10.1016/S0040-1951(98)00136-X.

Molnar, P. (1988), A review of geophysical constrain of the Himalaya on the deep structure of the Tibetan Plateau, the Himalaya and the Karakoram, and their tectonic implications, *Philos T. Roy. Soc. A* **326**, 1589, 33-88, DOI: 10.1098/rsta.1988.0080.

Nelson, K.D., and W.J. Zhao (1996), Partially molten middle crust beneath southern Tibet: Synthesis of Project INDEPTH Results, *Science* **274**, 5293, 1684-1688, DOI: 10.1126/science.274.5293.1684.

Rogers, J.W. (2004), *Continents and Supercontinents*, Oxford University Press, Oxford.

Royden, L.H., B. Clark, R.W. King, E. Wang, Z.L. Chen, F. Schen, and Y.P. Liu (1997), Surface deformation and lower crustal flow in eastern Tibet, *Science* **276**, 5313, 788-790, DOI: 10.1126/science.276.5313.788.

Schoenbohm, L.M., B.C. Burchfiel, and L. Chen (2006), Propagation of surface uplift, lower crustal flow, and Cenozoic tectonics of the southeast margin of the Tibetan Plateau, *Geology* **34**, 10, 813-816, DOI: 10.1130/G22679.1.

Spector, A., and F.S. Grant (1970), Statistical models for interpreting aeromagnetic data, *Geophysics* **35**, 2, 293-302, DOI: 10.1190/1.1440092.

Telford, W.M., L.P. Geldart, and R.E. Sheriff (1990), *Applied Geophysics*, Cambridge University Press, Cambridge.

Unsworth, M.J., A.G. Jones, W.B. Wei, G. Marquis, S.G. Gokan, and J.E. Spratt (2005), Crustal rheology of the Himalaya and Southern Tibet inferred from magnetotelluric data, *Nature* **438**, 7064, 78-81, DOI: 10.1038/nature04154.

Wang, C.Y., W.B. Han, J.P. Wu, H. Lou, and W.W. Chan (2007), Crustal structure beneath the eastern margin of the Tibetan Plateau and its tectonic implications, *J. Geophys. Res.* **112**, B7, B07307, DOI: 10.1029/2005JB003873.

Xiao, X.C. (2010), *Collision Orogeny and its Effect of Qinghai-Tibet Plateau*, Geological Publishing House, Beijing (in Chinese).

Xu, Z.Q., J.S. Yang, H.B. Li, J.X. Zhang, and C.L. Wu (2007), *Orogenic Plateau*, Geological Publishing House, Beijing (in Chinese).

Yang, W.C. (1985), The power spectrum analysis of the field data (A), Comp. *Techn. Geophys. Geochem. Explor*. **7**, 3, 188-196 (in Chinese).

Yang, W.C. (2009), Tectonophysics in Paleo-Tethys domain. **In:** Chapter 7, Petroleum IndustryPress, Beijing (in Chinese).

Yang, W.C., and A.Y. Guo (1979), Interpretation of gravity anomalies in frequency domain (A), *Technol. Geophys. Geochem. Prospect*. **79**, 1-16 (in Chinese).

Yang, W.C., and C.Q. Yu (2014a), Continental collision process reveled by world-wide comparison of crust and upper mantle structures (I), *Geol. Rev*. **60**, 2, 237-259 (in Chinese) .

Yang, W.C., and C.Q. Yu (2014b), Continental collision process revealed by worldwide comparison of crust and upper mantle structures (II), *Geol. Rev*. **60**, 3,486-502 (in Chinese).

Yang, W.C., Z.Q. Shi, Z.Z. Hou (2001), Discrete wavelet transform for multiple decomposition of gravity anomalies, *Chinese J. Geophys*. **45**, 4, 467-476.

Yang, W.C. J.R. Xu, Z.Y. Chen, and Z.Z. Hou (2005), *Regional Geophysics and Crust-mantle Interaction in Sulu-Dabie Orogenic Belt*, Geological Publishing House, Beijing, 161 pp. (in Chinese).

Zeng, L., L.E. Gao, K.J. Xie, and J.L. Zeng (2011), Mid-Eocene high Sr/Y granites in the Northern Himalayan Gneiss Domes: Melting thickened lower continental crust, *Earth Planet. Sci. Lett.* **303**, 3-4, 251-266, DOI: 10.1016/j.epsl.2011.01.005.

Zhao, G.Z., X.B. Chen, L.F. Wang, J.J. Wang, J. Tang, Z.S. Wan, J.H. Zhang, Y. Zhan, and Q.B. Xiao (2008), Evidence of crustal 'channel flow' in the eastern margin of Tibetan Plateau from MT measurements, *Chinese Sci. Bull.* **53**, 12, 1887-1893, DOI: 10.1007/s11434-008-0081-3.

Received 3 March 2015
Received in revised form 15 September 2015
Accepted 2 October 2015